NIRSPEC

UCLA Astrophysics Program **U.C. Berkeley** **W.M. Keck Observatory**

Don Figer **June 10, 1996**

NIRSPEC Optics Design Note 11.00
System Wavefront Error Budget (WFEB)

I. Introduction

The system wavefront error budget (WFEB) accounts for all the individual contributors to the WFE, and compares the total to that required to satisfy the image performance goal. Constructing the final WFEB is an interactive procedure requiring that various trade-offs be considered, i.e. cost versus performance. The model described in this document was used to optimize the design specifications so that the overall performance specification was met, while the ease of manufacturing and assembly were maximized.

II. Constructing the WFEB

As stated elsewhere, the image performance goal is 80% ensquared energy in one spectrometer pixel (enpixelled energy, EPE). In order to complete the WFEB, this image performance goal must be translated into a statement of total WFE. Unfortunately, this is not so easy, and it requires empirical knowledge of previously-built systems. The general difficulties in constructing the WFEB are discussed below.

A. Parametrization of WFE

The wavefront error is often expressed as the RMS deviation from a perfect wavefront over the whole beam for a given field point. This parametrization has the advantages that it is easy to add individual contributions together, it is relatively easy to measure, and it is a single number. Unfortunately, there is no general transformation between EPE and RMS WFE, i.e. two systems with identical total WFE_{RMS} may give different EPE values. This is due to the fact that WFE_{RMS} does not include any information about the power spectrum of the wavefront deviations. In other words, the peak-to-valley amplitudes and frequencies of the wavefront deviations can have an important effect on the final image quality.

The resolution to this difficulty relies on empirical knowledge of existing optical systems. For instance, manufacturers have seen that systems containing a TMA will tend to have image performance which scales in some well-behaved way with the total system wavefront error. This is true because these systems have total errors dominated by the TMA design residual and fabrication errors. With this relation, then, we can translate the total WFE into EPE, first making sure that the system is dominated by error in manufacturing the TMA.

B. Estimating individual contributions

One difficulty in developing the WFEB is that some classes of errors are not well known. For instance, how much error will result from differential thermal contraction? How about misalignments? These effects can be approximated from theoretical expectations or empirical knowledge, or they can modeled in Zemax with considerable effort. We tried to use the experience of vendors to estimate such contributions, but in some cases, we resorted to modeling.

C. WFE as a function of field location at the final focus

The WFE due to the TMA will be a strong function of field location at the TMA focal plane. Because the TMA dominates the WFEB, this effect controls the total error over most of the field regardless of other effects, i.e. image rotator position or slit position.

D. WFE as a function of slit position

Both the front-end design and the back-end collimator design will introduce WFE which depends on field location in the slit. At the center of the TMA field of view, this effect will dominate the errors. The TMA errors dominate most of the field outside of the center, so the difference between the center and edge of the slit will be relatively smaller over this area. See Figure 1 for the variation of WFE along the slit.

There is an even more troublesome effect in that the WFE will depend strongly on which edge of the slit is considered. There seems to be very little difference in which slit edge is chosen for the front-end alone, but it can change the WFE by a factor of 3 for the end-to-end values. About half of this difference is due to the fact that the back-end collimator will induce different amounts of WFE depending on which side of the slit the field point is on. The rest of the difference is due to asymmetries in the TMA.

E. WFE as a function of image rotator position

The front-end design is fairly well-corrected for the nominal image rotator position; however, this correction gets worse for larger image rotator angles. This effect has no impact for the central field point where the imaging is perfect for all rotator angles. Figure 1 shows this effect at the slit focal plane.

F. Non-random addition of errors

Individual wavefront errors might not add in quadrature. A good illustration of this effect can be seen in the front-end optics. We could estimate individual contributions to the total WFE error due to the two K-mirror assemblies. We could then add these values in quadrature, but this would be a horrible estimate of how the two assemblies would perform together. As previously stated, the errors will add or cancel depending on the orientation of the assemblies with respect to each other. For this reason, it is sometimes best to figure the induced WFE of whole assemblies or trains.

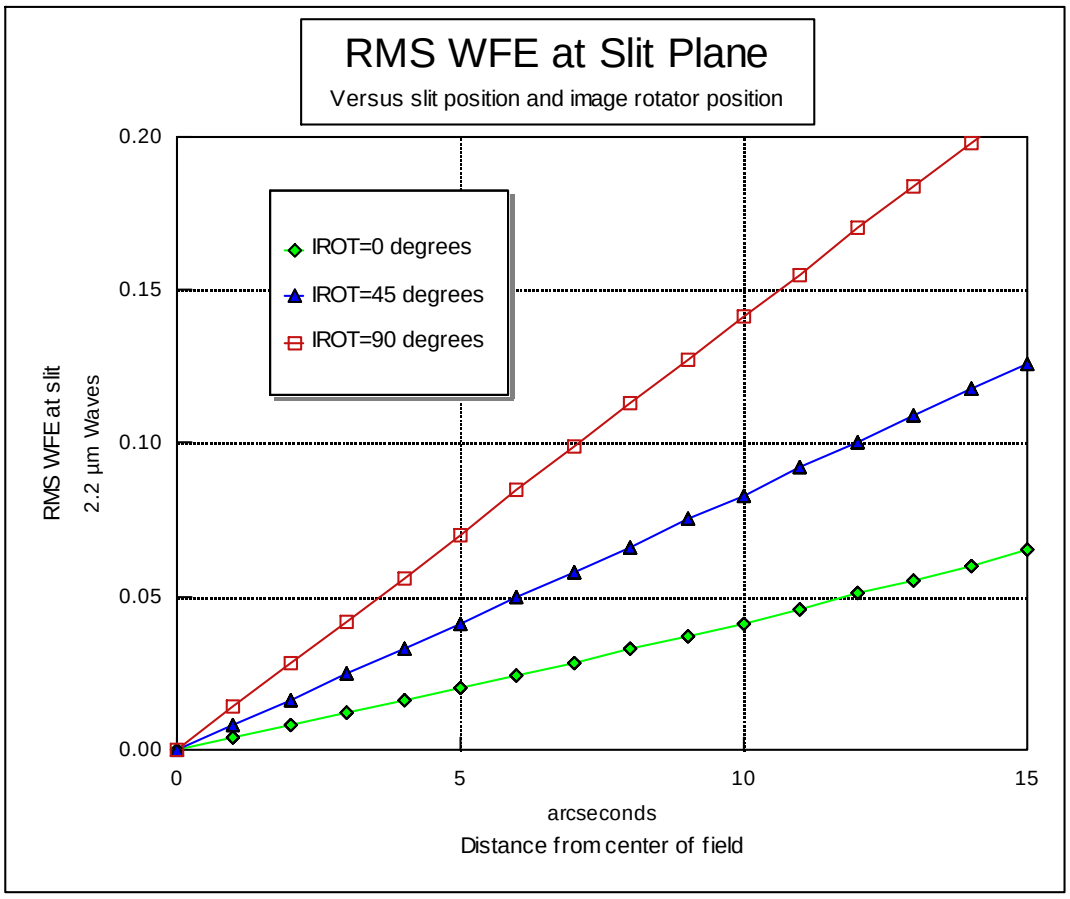

Figure 1. RMS WFE as a function of slit position and image rotator position in the front end.

III. Sources of Wavefront Error

Just as the wavefront errors are deviations from ideal, the classes of errors can be thought of as deviations from perfect design, fabrication, and construction of the system. The first source of error is known as the ***design residual***. This error can be seen in the optical design itself and gives a lower-limit to the total error for the system after it has been built. The second source of error is due to surface ***irregularity***. Here, the optical surfaces deviate from their ideal prescriptions. Sometimes, the misfigure can be decomposed into a power term and a higher frequency term. The latter is usually called irregularity and the former is often called surface accuracy or surface figure. In this document, I regard all deviations, regardless of the power spectrum, as surface irregularity. Once the mirrors are made, they must be held in their mounts. There will be induced wavefront error in as much as these mounts affect the optical surfaces; I call this ***mount*** error. The mounted optics then need to be aligned with respect to each other. Misalignments will result in ***alignment*** error. Even after construction, there is a possibility that the errors above will change when the assembly is cooled down to operating temperature. These changes could be stuffed into the above categories where appropriate, but I have broken them out into the ***environment*** category. The last source of error lumps all of our measurement uncertainty into one category, ***data measurement***. This might be due

to measurement error in determining the realized alignment, surface figure, or any of the other errors.

IV. The WFE Table

The WFE table for NIRSPEC is shown in Figure 3, where the numbers represent an "averaged" case. The 9 field points (wavelengths), used to construct this average, are shown schematically in Figure 2. Individual elements and assemblies are listed in the rows, and the error classes are listed along the columns. The values in the table are peak-to-valley (PV), unless noted otherwise. They are in fractions of helium-neon laser waves (λ_{HeNe} = 0.6328 μm); this type of monochromatic light is usually used in testing optics.

The irregularity values are translated into induced WFE ("cont to WFE" column). The design residuals are broken out into 5 different cases: center of slit:θ_{IROT}=0°, slit edge: 0°, slit edge:22.5°, slit edge:45°, and slit edge:90°. The "align.", "mount", "env.", and "data meas." columns contain the induced WFE as described in the discussion above. The last 5 columns contain the quadrature sum of the previous columns where values for the 5 different cases are shown.

Assembly errors are either quadrature sums of errors for individual elements in the assembly or were directly taken from Zemax. Intermediate totals for the front-end and back-end are given; these values are quadrature sums. The end-to-end (ETE) design residuals are actually measured from the model, and thus do not represent the quadrature sum of the front-end and back-end values. $WFE_{ETE\text{-}RMS}$ values are computed by dividing the $WFE_{ETE\text{-}PV}$ values by a conversion factor, in this case, 5. I find that this ratio is used by some of the vendors and is confirmed in Zemax for our system. The ESE in 1 pixel (EPE) is shown in the 5 last columns on the right. The conversion from WFE_{RMS} to EPE was taken from SSG, Inc., documentation and will be discussed in a later section.

A. Design Residual

The design residual is simply the induced WFE due to the fact that the design is intrinsically imperfect. In some cases, a practical optical design can be essentially perfect, i.e. an off-axis parabola (OAP) for the central field point. Such a design would have zero design residual and induce no WFE. In fact, we have employed 3 consecutive OAPs in NIRSPEC, and this is reflected in the "0,0" column. There are no design residuals all the way through the 3 OAPs, and up to the TMA, for the central field position.

For off-axis field points, the front-end does have some design residual. The amount depends upon image rotator position. Figure 1 gives a graphical representation of the design residuals in the front-end for various image rotator positions and field points. Notice that the residuals are RMS and are expressed in terms of 2.2 μm waves in that figure. To convert these into PV values expressed in 0.6328 μm waves, as in Figure 3, just scale the values in the graph by 17.4. The design satisfies the Rayleigh criterion (WFE_{PV} < 0.25λ) for diffraction-limited systems up to 120, 60, and 40, in radius, at θ_{IROT}=0°, 45°, and 90° respectively for λ = 2.2 μm. The diffraction-limited field sizes at 1.1 μm are about half of these values.

I have not broken out individual design residuals for the OAPC because these values do not add in quadrature with downstream design residuals from the other elements. This phenomenon can also be seen by examining the end-to-end design residuals; they are not simply quadrature sums of the front-end and back-end residuals. Notice, for instance, that the value for the end-to-end model for the "edge, 90°" case is less than the value for just the front-end. Clearly, the back-end and front-end are working together to cancel some aberrations.

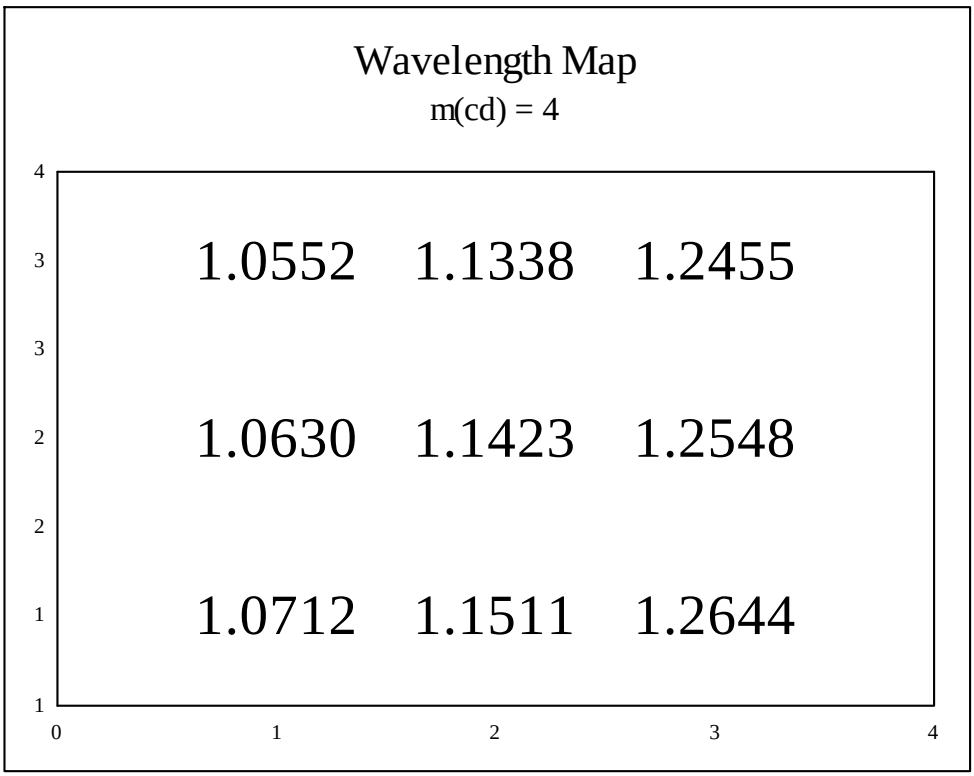

Figure 2. Wavelength map for extreme fields points on the array. Three echelle orders are represented, and the cross-disperser is used in 4th order.

Figure 4 gives the WFE values measured from the Zemax end-to-end model. The tables include values at the 9 field points depicted in Figure 2. Cases for 4 different image rotator positions (0°, 22.5°, 45°, and 90°) and 3 extreme slit positions (+edge=+150 and ! edge= ! 150) are included.

WFE in HeNe Waves (PV)

			cont	center	edge	edge	edge	edge				data	center	edge	edge	edge	edge
		IRR	to WFE	0°	0°	22.5°	45°	90°	align.	mount	env.	meas.	0°	0°	22.5°	45°	90°
window		0.10	0.10														
IROT	flat1	0.10	0.20														
	OAP1	0.10	0.20														
	flat2	0.10	0.20														
sub total			0.35						0.26	0.35	0.25	0.25					
filter		0.10	0.10														
FCON	flat3	0.10	0.20														
	OAP2	0.10	0.20														
	flat4	0.10	0.20														
sub total			0.35						0.26	0.35	0.25	0.25					
Front-end			0.51	0.00	1.07	1.40	2.10	3.53	0.37	0.49	0.35	0.35	0.94	1.43	1.69	2.31	3.65
OAPC		0.20	0.40						0.03	0.00	0.25	0.25					
echelle		0.20	0.40						0.00	0.00	0.25	0.00					
cross-disperser		0.20	0.40						0.00	0.00	0.25	0.00					
TMA	prim.	0.25	0.50														
	sec.	0.25	0.50														
	tert.	0.25	0.50														
sub total			0.87						0.63	0.00	1.61	0.25					
Back-end			1.11	1.90	2.39	2.39	2.39	2.39	0.63	0.00	1.67	0.35	2.85	3.20	3.20	3.20	3.20
End-to-end (PV)			1.22	1.90	2.57	2.29	2.41	3.40	0.73	0.49	1.70	0.50	3.00	3.47	3.27	3.35	4.12
End-to-end (RMS)			0.24	0.38	0.51	0.46	0.48	0.68	0.15	0.10	0.34	0.10	0.60	0.69	0.65	0.67	0.82
												EPE =	77%	72%	74%	73%	65%

Figure 3. WFE table for an "average" case (see Figure 4). The averages account for 9 field points distributed evenly in a 3X3 pattern across the TMA. The values at the "slit edge" are averages between the values for either edge of a 300 slit as shown in Figure 4. The final end-to-end WFE is given at the bottom, expressed in PV and RMS. The total "enpixelled" energy (EPE) is given in the lower right corner. See the text for a discussion of the relation between WFE and EPE.

TMAKCK21

0°

lambda	WFE RMS (lambdas)	WFE RMS (µm)	WFE RMS HeNe	WFE PV HeNe
1.2548	0.248	0.311	0.49	2.46
1.2644	0.268	0.339	0.54	2.68
1.2455	0.270	0.336	0.53	2.66
1.1423	0.100	0.114	0.18	0.90
1.1511	0.124	0.143	0.23	1.13
1.1338	0.248	0.281	0.44	2.22
1.0630	0.135	0.144	0.23	1.13
1.0712	0.220	0.236	0.37	1.86
1.0552	0.231	0.244	0.39	1.93
average		0.24	0.38	1.89

+edge

	0°				22.5°				45°				90°			
	WFE RMS (lambdas)	WFE RMS (µm)	WFE RMS HeNe	WFE PV HeNe	WFE RMS (lambdas)	WFE RMS (µm)	WFE RMS HeNe	WFE PV HeNe	WFE RMS (lambdas)	WFE RMS (µm)	WFE RMS HeNe	WFE PV HeNe	WFE RMS (lambdas)	WFE RMS (µm)	WFE RMS HeNe	WFE PV HeNe
1.2548	0.225	0.282	0.45	2.23	0.174	0.218	0.35	1.73	0.165	0.207	0.33	1.64	0.259	0.325	0.51	2.57
1.2644	0.424	0.536	0.85	4.24	0.415	0.525	0.83	4.15	0.491	0.621	0.98	4.91	0.601	0.760	1.20	6.00
1.2455	0.352	0.438	0.69	3.46	0.299	0.372	0.59	2.94	0.278	0.346	0.55	2.74	0.358	0.446	0.70	3.52
1.1423	0.153	0.175	0.28	1.38	0.113	0.129	0.20	1.02	0.142	0.162	0.26	1.28	0.295	0.337	0.53	2.66
1.1511	0.168	0.193	0.31	1.53	0.175	0.201	0.32	1.59	0.224	0.258	0.41	2.04	0.379	0.436	0.69	3.45
1.1338	0.272	0.308	0.49	2.44	0.281	0.319	0.50	2.52	0.328	0.372	0.59	2.94	0.464	0.526	0.83	4.16
1.0630	0.253	0.269	0.42	2.12	0.172	0.183	0.29	1.44	0.133	0.141	0.22	1.12	0.245	0.260	0.41	2.06
1.0712	0.277	0.297	0.47	2.34	0.271	0.290	0.46	2.29	0.300	0.321	0.51	2.54	0.451	0.483	0.76	3.82
1.0552	0.295	0.311	0.49	2.46	0.227	0.240	0.38	1.89	0.168	0.177	0.28	1.40	0.186	0.196	0.31	1.55
average		0.312	0.493	2.467		0.275	0.435	2.175		0.290	0.458	2.288		0.419	0.662	3.310

-edge

	0°				22.5°				45°				90°			
	WFE RMS (lambdas)	WFE RMS (µm)	WFE RMS HeNe	WFE PV HeNe	WFE RMS (lambdas)	WFE RMS (µm)	WFE RMS HeNe	WFE PV HeNe	WFE RMS (lambdas)	WFE RMS (µm)	WFE RMS HeNe	WFE PV HeNe	WFE RMS (lambdas)	WFE RMS (µm)	WFE RMS HeNe	WFE PV HeNe
1.2548	0.290	0.364	0.58	2.88	0.322	0.404	0.64	3.19	0.377	0.473	0.75	3.74	0.508	0.637	1.01	5.04
1.2644	0.278	0.352	0.56	2.78	0.252	0.319	0.50	2.52	0.270	0.341	0.54	2.70	0.374	0.473	0.75	3.74
1.2455	0.212	0.264	0.42	2.09	0.256	0.319	0.50	2.52	0.307	0.382	0.60	3.02	0.398	0.496	0.78	3.92
1.1423	0.224	0.256	0.40	2.02	0.169	0.193	0.31	1.53	0.176	0.201	0.32	1.59	0.317	0.362	0.57	2.86
1.1511	0.253	0.291	0.46	2.30	0.187	0.215	0.34	1.70	0.181	0.208	0.33	1.65	0.305	0.351	0.55	2.77
1.1338	0.408	0.463	0.73	3.66	0.344	0.390	0.62	3.08	0.310	0.351	0.56	2.78	0.337	0.382	0.60	3.02
1.0630	0.249	0.265	0.42	2.09	0.200	0.213	0.34	1.68	0.217	0.231	0.36	1.82	0.371	0.394	0.62	3.12
1.0712	0.376	0.403	0.64	3.18	0.305	0.327	0.52	2.58	0.266	0.285	0.45	2.25	0.315	0.337	0.53	2.67
1.0552	0.367	0.387	0.61	3.06	0.341	0.360	0.57	2.84	0.359	0.379	0.60	2.99	0.507	0.535	0.85	4.23
average		0.338	0.534	2.672		0.304	0.481	2.405		0.317	0.501	2.504		0.441	0.697	3.484

Figure 4. End-to-end design residuals for various image rotator positions and slit positions. There are 9 wavelengths corresponding to 9 evaluation points at the focal plane. Some of the most extreme field points lie off the detector. The top set of numbers correspond to the center of the slit. The next 2 sets correspond to the positive edge ("+edge") of the slit and the negative edge (" ! edge") of the slit. The slit length is 300.These same values are all shown graphically in Figures 5-8.

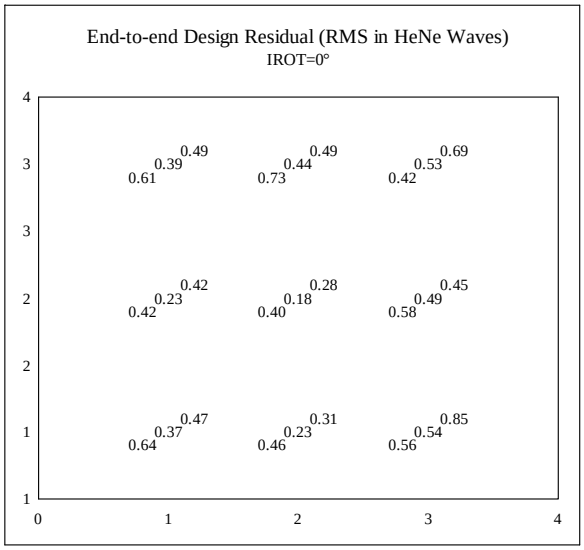

Figure 5

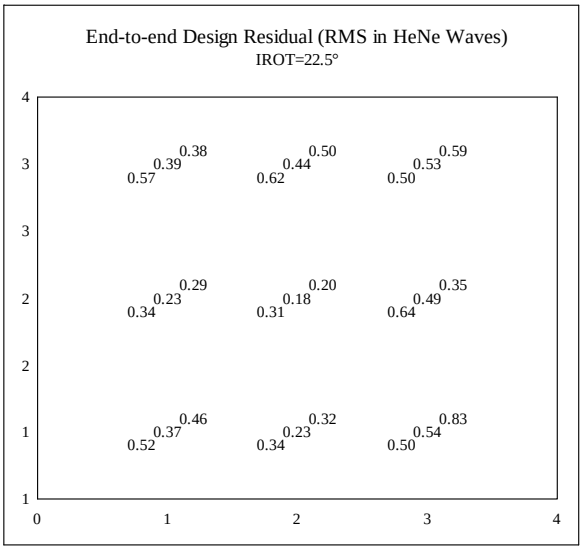

Figure 6

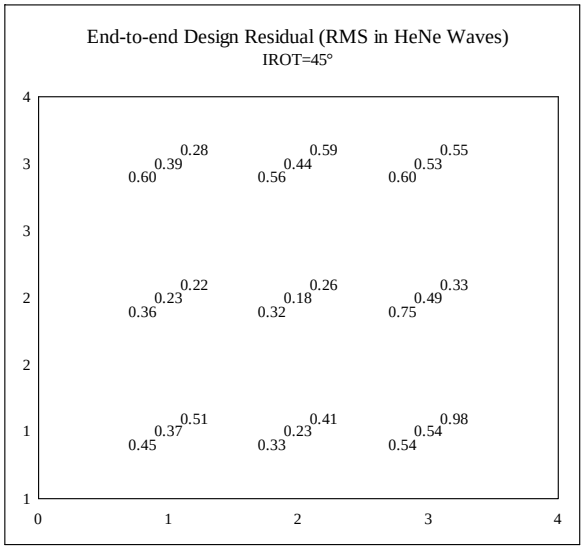

Figure 7

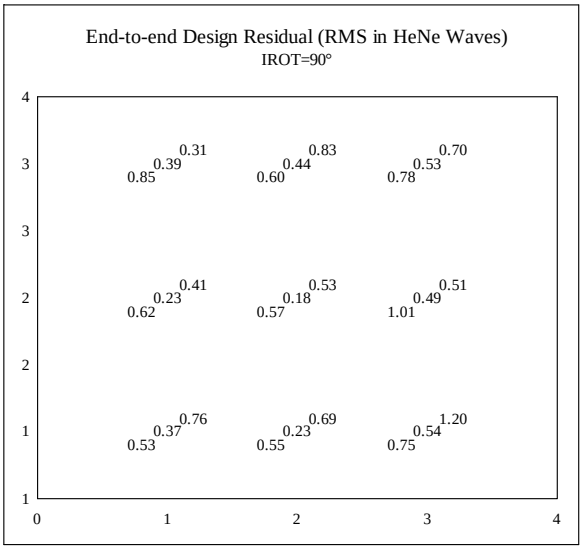

Figure 8

Figures 5 through 8 give the design residuals (RMS in $\mathbf{8}_{\mathrm{HeNe}}$ waves) for various field points and slit positions. The different figures are for different image rotator (IROT) positions as shown in the second title of each graph. Each diagram gives values for 9 locations at the focal plane; the values on the axis labels are meaningless. There are 3 values for each field point corresponding to the center and both edges of the slit. Notice that some of the values, for a given field point and slit position, are smallest for IROT ... 22.5°. Also, notice that the values for the central slit positions are invariant to a change in image rotator position. Some of the extreme locations actually fall outside of the array.

B. Irregularity (IRR)

The allotted IRR is strongly dependent on what manufacturers can make. It also depends on the thermal stability of the surface. In our WFEB, we usually tabulate thermally induced WFE in the environmental column. Contrary to this, however, we do not allow any surface degradation due to thermal effects when assigning the allowable induced WFE due to IRR. This means that an optic must maintain its IRR spec as indicated in the WFEB at cold temperatures.

For the window, we can calculate the total induced WFE by summing the individual contributions from each of the two surfaces. Assuming that we can expect a surface figure of $\lambda_{HeNe}/10$ PV, we will get a contribution of $(\lambda_{HeNe}/10)\times(n_{CaFl} - n_{air/vac})$ to the WFE per surface. The window, then, will contribute $< \lambda_{HeNe}/10$ total WFE. In this case, I have simply added the induced errors from the front surface and the back surface. We could have added in quadrature instead. This would have given a smaller induced error. In any case, the allotted error is an upper bound, assuming that a manufacturer can provide this level of flatness. Recall that the figures in the WFEB are always determined over the beam width. For the window, the beam will be less than a few mm. We can expect that a manufacturer will be able to produce a window with flatness better than $\lambda_{HeNe}/10$ for any few mm subaperture.

We require $\lambda_{HeNe}/10$ PV IRR on all of the front-end elements. Of course, this requirement is most stringent for the flats nearest the pupil image, flat2 and flat3. The beam is largest at these locations, with d_{beam} - 27 mm, or - 70% (80%) of the short dimension on the flat2 (flat3). The requirement should be quite easily met at the two other flats owing to the small beam size, d_{beam} - 7 mm at flat1 and 5 mm at flat4, or - 10% of the short dimension on both flats. At both OAPs, the beam size is - 27 mm, or - 70% (85%) of the diameter of OAP1 (OAP2). Finally, we should be able to obtain filters with this IRR.

The OAPC has been given a factor of 2 greater IRR, $\lambda_{HeNe}/5$ PV, than the upstream elements. This is in acknowledgment of the fact that the beam size is very large at the OAPC, $d_{beam} = 120$ mm. It will be very challenging to achieve even this relaxed IRR.

The echelle and cross-disperser have been allotted IRR $< \lambda_{HeNe}/5$ PV. Again, the beam spans nearly the whole blank size, thus requiring that this spec be held over linear dimensions as large as 310 mm. The final surface figure on these pieces will be determined by the flatness of the master ruling and the bi-metallic effect as the gratings cool down. We know that the master ruling for the echelle has produced gratings in the past with less than our specified IRR; this can be seen in interferograms sent to us by Spectronic, Inc. We will also require that the grating substrates be heavily de-stressed and heat treated so that they will maintain their shape at temperature. The bi-metallic effect is a bit more difficult to combat. This effect derives from the different coefficients of thermal expansion for the aluminum and the ruling glue. It is difficult to control this because we do not have any freedom in choosing a glue with ideal properties. We will have to hope that this effect does not induce extra WFE.

IRR on the TMA surfaces has greater impact on performance than the IRR on any other surface. Because of manufacturing limits, we had to choose between IRR < $\mathbf{8}_{HeNe}$/2 PV and IRR < $\mathbf{8}_{HeNe}$/4 PV surfaces. The difference in cost is significant, and so is the difference in performance, as we will see later. At this point, suffice it to say that we chose the tighter requirement, IRR < $\mathbf{8}_{HeNe}$/4 PV.

C. Mount Error

We only assess mount error in the front-end mirrors because we have confidence that the mounts will be stress-free in the back-end elements. The numbers in the front-end are somewhat pessimistic, but we used vendor response to figure them. With proper care, we might be able to zero out these entries. For instance, a single point mount on the flat mirror prism (furthest from both surfaces) would probably have no effect on the optical surfaces.

D. Alignment Error

The alignment errors were assessed by perturbing the various elements the maximum allowable amount without violating the alignment tables. The entry for the TMA was taken from vendor input.

E. Environment Error

These values were taken from vendor input. Recall that we are not allowing any surface degradation due to thermal effects. In other words, the surface figures must be maintained at temperature, and we will only allow induced WFE from thermal effects due to changes in alignment.

F. Data Measurement

These values are consistent with typical interferometers at vendors.

V. The Relationship between System WFE and EPE

SSG, Inc., has indicated to us that the total system WFE is related to the final EPE by a linear relationship. I have fit a line to data points from their documentation to produce Figure 9. Here, we can see the expected trend of higher WFE giving lower EPE. It is important to realize that this relationship is only valid over the range indicated. For very small WFE values, the system WFE is probably dominated by sources other than the TMA.

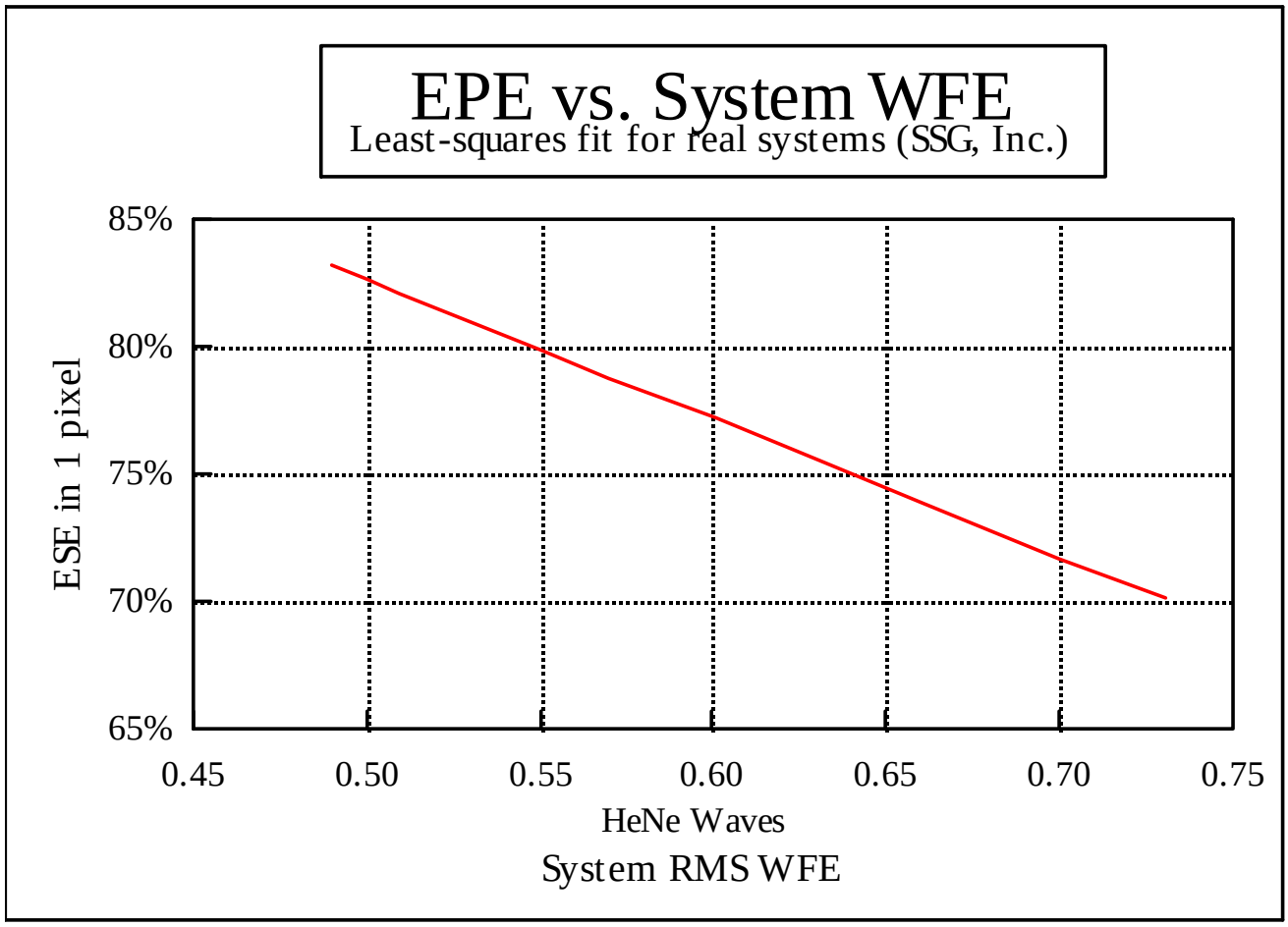

Figure 9. Empirical average relationship for TMA systems manufactured by SSG, Inc.

This relationship gives us the opportunity to recast Figures 5 through 8 in terms of EPE instead of system WFE. These values are shown in Figures 10 through 13. Here we can see that the EPE decreases away from the center of the array and away from the center of the slit for individual field points.

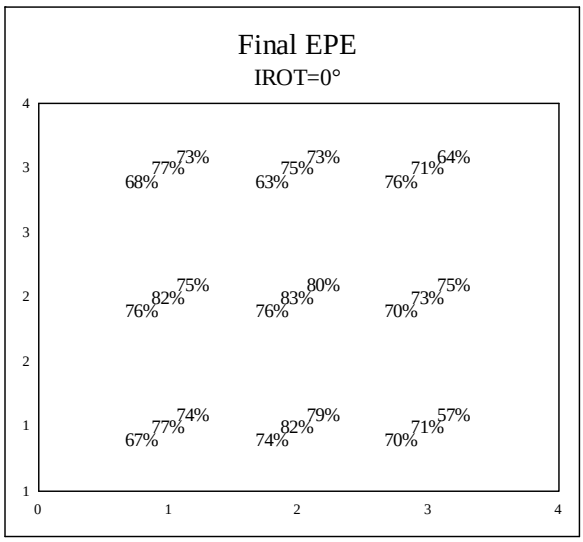

Figure 10

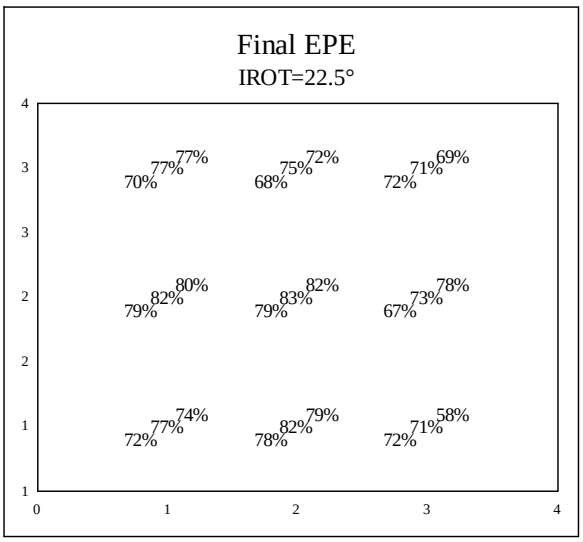

Figure 11

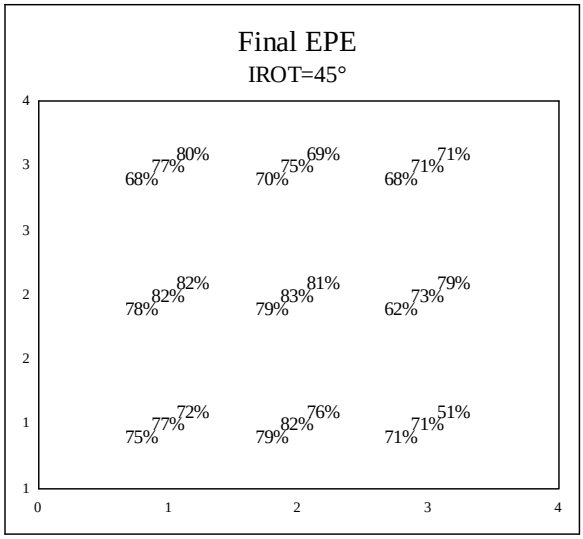

Figure 12

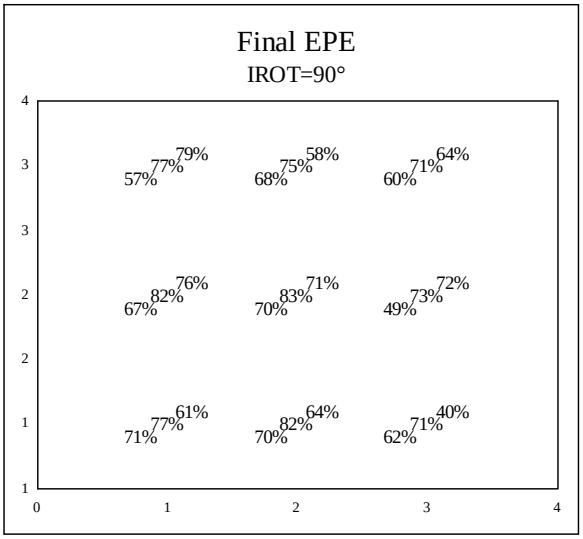

Figure 13

Figures 10 through 13 give the EPE for various field points and slit positions. The different figures are for different image rotator (IROT) positions as shown in the second title of each graph. Each diagram gives values for 9 locations at the focal plane; the values on the axis labels are meaningless. There are 3 values for each field point corresponding to the center and both edges of the slit. Notice that some of the values for a given field point and slit position are highest for IROT=22.5°. Also, notice that the values for the central slit positions are invariant to a change in image rotator position. Some of the extreme locations actually fall outside of the array.

VI. The Consequences of TMA Surface Figure on EPE

You will notice in Figure 3 that we specified $\mathbf{8}_{HeNe}/4$ PV for surface irregularity in the TMA surfaces. We probably spent as much effort determining these values as we spent in constructing the WFEB itself. That is because this level of irregularity is very difficult to achieve on these types of surfaces. In fact, we could have specified $\mathbf{8}_{HeNe}/2$ PV and received a considerable discount in fabrication cost.

Instead, we examined the natural effects of higher irregularity on the final system performance. To do this, we used the relations previously described. In Figure 3, I have plotted the total system WFE versus TMA design residual for both irregularities. In the legend, "¼ Wave Optics" refers to using TMA surfaces with irregularities less than $\mathbf{8}_{HeNe}/4$ PV. This kind of plot shows us how much of the total WFE is due to TMA design residual, and how much is due to TMA surface irregularity. Notice that even in the case of zero TMA design residual, the total system WFE is non-zero; in fact, it is near $0.49\mathbf{8}_{HeNe}$ RMS for the ¼ wave case and near $0.56\mathbf{8}_{HeNe}$ RMS for the ½ wave case. This is simply a reflection of the fact that there are sources of error in the system other than TMA design residual. The important point is that the TMA surface irregularity amounts to over 15% of the system WFE. This is important because it indicates that reducing the irregularity on the TMA surfaces would be a very effective way to reduce the system WFE, and, in turn increase the EPE.

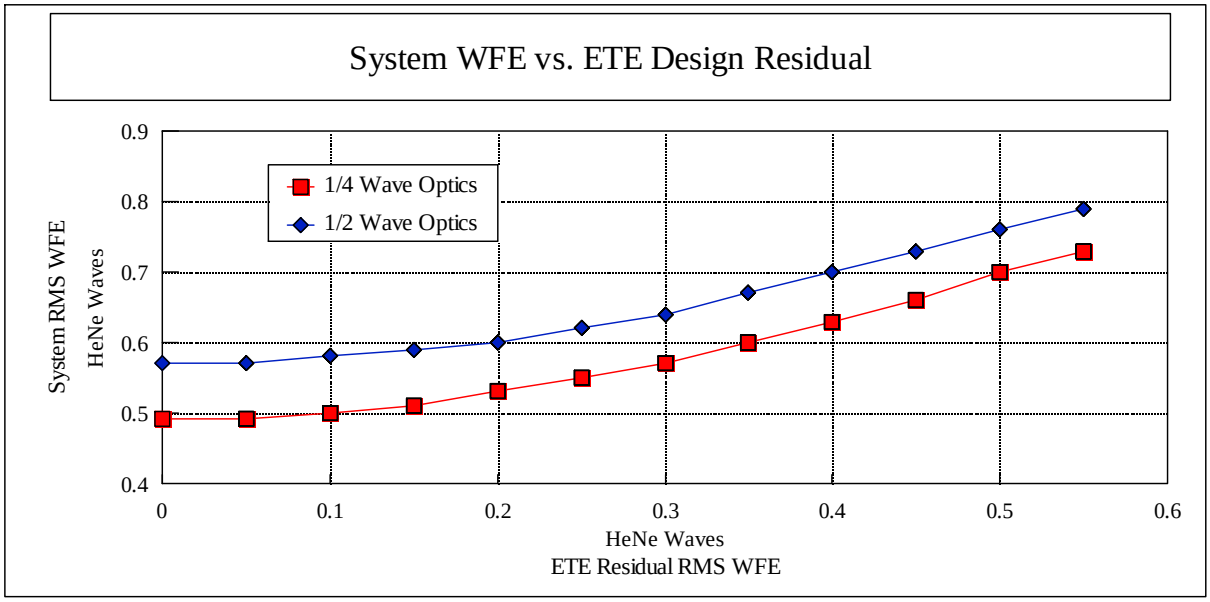

Figure 14. Relationship between system WFE and end-to-end design residual. These values are based upon the model in Figure 3. The "¼ wave optics" case assumes that the surface irregularity on the TMA elements is $< \mathbf{8}_{HeNe}/4$ PV. Notice that this assumption improves the system WFE by 15% over the "½ wave optics" case.

We can see the effect on EPE due to the surface irregularity on the TMA surfaces in Figure 15. Here, we can see that the EPE is increased by about 5-6% for the ¼ wave optics case over the ½ wave optics case. We can also see that the TMA design residuals do not dominate the performance for TMA design residuals below $\sim \lambda_{HeNe}/5$ RMS; note that the relationship between EPE and WFE is based upon errors being dominated by the TMA irregularity and design residuals. This figure shows us that it would be impossible to achieve our performance goal (80% EPE) anywhere in the focal plane using ½ wave optics. It also shows us that we could achieve the goal using ¼ wave optics for areas in the focal plane where the TMA design residual is $< \lambda_{HeNe}/4$ RMS. This condition is satisfied for a circle with radius about equal to 1/4 of the full array and centered at the center of the array.

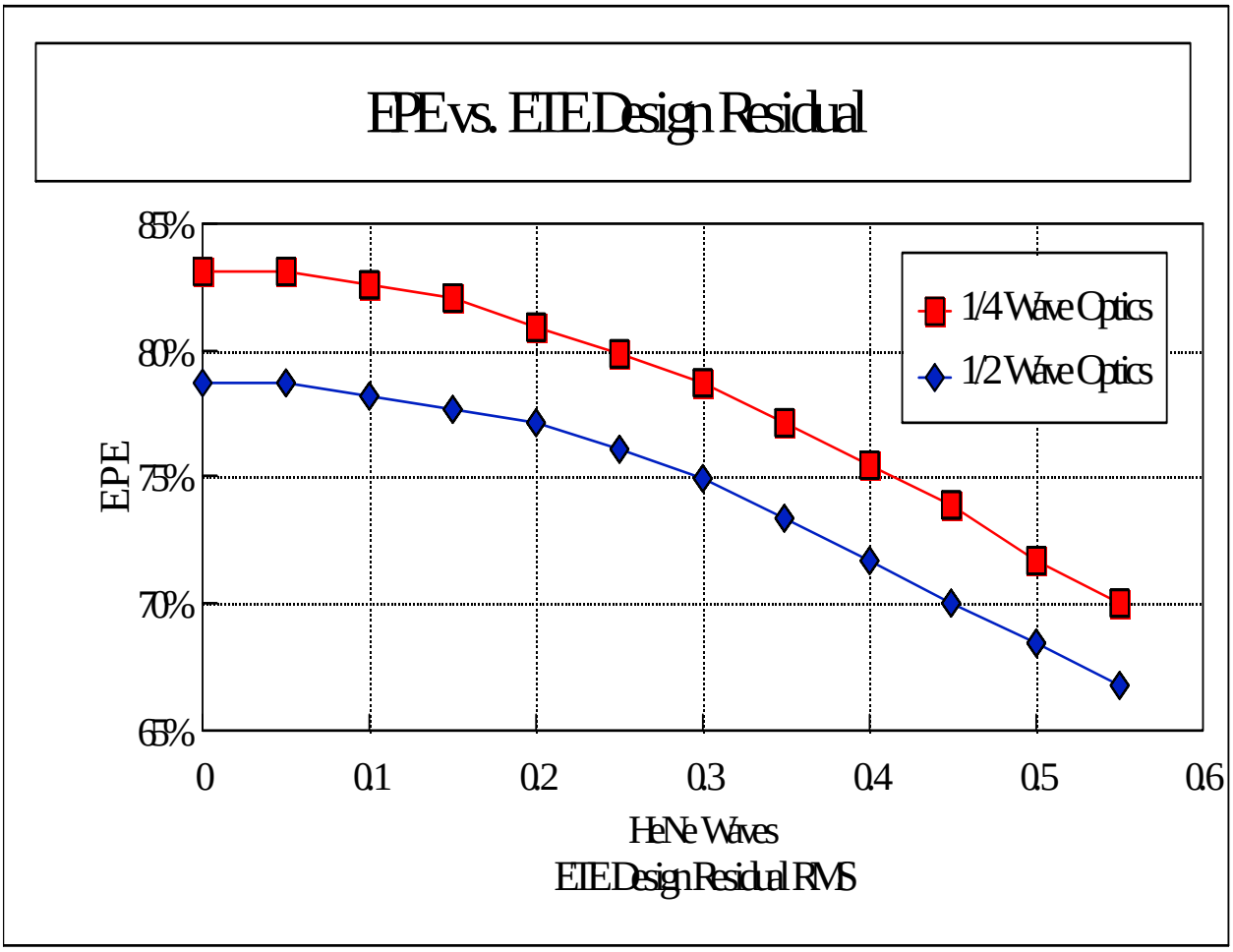

Figure 15. Relationship between EPE and end-to-end design residuals. These numbers are based upon the law in Figure 9, and the individual contributions to the total WFE, as given in Figures 3 and 14.